Atmos. Chem. Phys. Discuss., 8, 1549–1588, 2008
www.atmos-chem-phys-discuss.net/8/1549/2008/

Atmospheric Chemistry and Physics Discussions

A framework for comparing remotely sensed and in-situ CO_2 concentrations

R. Macatangay[1,2], T. Warneke[1], C. Gerbig[2], S. Körner[2], R. Ahmadov[2], M. Heimann[2], and J. Notholt[1]

[1]Institute of Environmental Physics, University of Bremen, Bremen, Germany
[2]Max Planck Institute for Biogeochemistry, Jena, Germany

Received: 22 November 2007 – Accepted: 13 December 2007 – Published: 29 January 2008

Correspondence to: R. Macatangay (macatang@iup.physik.uni-bremen.de)

Abstract

A framework that allows validating CO_2 column averaged volume mixing ratios (VMRs) retrieved from ground-based solar absorption measurements using Fourier transform infrared spectrometry (FTS) against measurements made in-situ (such as from aircrafts and tall towers) has been developed. Since in-situ measurements are done frequently and at high accuracy on the global calibration scale, linking this scale with FTS total column retrievals ultimately provides a calibration scale for remote sensing. FTS, tower and aircraft data were analyzed from measurements during the CarboEurope Regional Experiment Strategy (CERES) from May to June 2005 in Biscarrosse, France. Carbon dioxide VMRs from the MetAir Dimona aircraft, the TM3 global transport model and Observations of the Middle Stratosphere (OMS) balloon based experiments were combined and integrated to compare with FTS measurements. The comparison agrees fairly well with differences resulting from the spatial variability of CO_2 around the FTS as measured by the aircraft. Additionally, the Stochastic Time Inverted Lagrangian Transport (STILT) model served as a "transfer standard" between the in-situ data measured at a co-located tower and the remotely sensed data from the FTS. The variability of carbon dioxide VMRs was modeled well by STILT with differences coming partly from uncertainties in the spatial variation of carbon dioxide.

1 Introduction

There has been much evidence that increasing global temperatures for the past 50 years can be attributed to human activity and that anthropogenic influence would continue to change the composition of the atmosphere in the next years. Due to man's insatiable need for energy and industrialization, carbon dioxide (CO_2), a by-product of fossil fuel combustion and biomass burning (brought about by land use change) has become the most significant greenhouse gas (IPCC, 2005). Due to this, much attention is being given on the absorption characteristics of CO_2 as well as its contribution

to possible climate changes due to its increased concentration in the atmosphere (McCartney, 1983).

Currently, global transport models utilize in-situ measurements of carbon dioxide from a global network of surface sites for analyzing, estimating and predicting its concentrations as well as determining regional scale exchanges of CO_2 (Rödenbeck et al., 2006; Peylin et al., 2005; Peters et al., 2007). These in-situ surface measurements have the advantage that they are highly accurate. However, they have a limited spatial coverage and an increasing number of measurements are performed within the proximity of local sources and sinks with networks of tall tower observatories over the continents. This makes model estimates susceptible to transport errors, such as errors in vertical transport processes (moist convection and turbulent mixing in the boundary layer), especially for continental regions (Washenfelder et al. 2006; Gerbig et al. 2007). This, in turn, provides uncertainties in the geographic (spatial) and temporal distributions of CO_2 sources and sinks (Dufour et al., 2004; Gerbig et al., 2007). The uncertainties imply that difficulties would come about in predicting the response of carbon dioxide due to climate and land-use changes (Yang et al., 2002), as well as in projecting the future rate of increase of atmospheric CO_2 (Dufour et al., 2004).

Space-borne or satellite measurements, such as the Orbiting Carbon Observatory (OCO) (whose planned launch is in 2009) (Crisp et al., 2004), the Scanning Imaging Absorption Spectrometer for Atmospheric Chartography (SCIAMACHY) (Burrows et al., 1990) and the Greenhouse Gases Observing Satellite (GOSAT), may offer the solution to the problem of sparse spatial and temporal distributions of carbon dioxide sources and sinks by providing global column measurements of CO_2 (Yang et al., 2002). To supplement and validate the satellite data, ground-based solar absorption spectroscopy in the infrared or Fourier transform infrared (FTIR) spectrometry is employed (Warneke et al., 2005). It measures the same quantity (column concentrations) as the satellite and exhibits less spatial and temporal variability as compared to in-situ data while retaining information about the surface fluxes and the diurnal behavior of carbon dioxide. It also complements existing in-situ networks and provides information

about CO_2 exchange on regional scales (Washenfelder et al., 2006). The Total Carbon Column Observing Network (TCCON), which is a system of high-resolution ground-based FTIR spectrometers, provides this capability (http://www.tccon.caltech.edu/).

In this paper, CO_2 column abundances from solar absorption FTIR measurements during the CarboEurope Regional Experiment Strategy (CERES) in Biscarrose, France are presented as well as a method to calibrate these measurements against aircraft data. To provide for a "transfer standard" between incomparable measurement techniques, such as in-situ tower data and column concentrations from FTIR measurements, the Stochastic Time Inverted Lagrangian Transport (STILT) model (Lin et al., 2003) was utilized. The study is not about showing the full capability of solar absorption FTIR measurements for column retrievals of CO_2, since the instrument used in CERES is inferior to the ones targeted and in operation for TCCON. The main aim is to provide a framework that allows validating the FTIR retrievals against measurements made in-situ from aircraft as well as from tall towers. Such in-situ measurements are made regularly with high accuracy on the global calibration scale, and linking this scale with FTIR retrievals ultimately provides a calibration scale for remote sensing.

2 Determining CO_2 concentrations

Fourier transform infrared (FTIR) spectroscopy measurements were performed during the CarboEurope Regional Experiment Strategy (CERES) from May to June 2005. CERES aims to come up with a comprehensive database of atmospheric CO_2 concentrations, fluxes, as well as meteorological parameters at the regional scale. An overview of the experiment is given in Dolman et al. (2006). The experiment area is a 250 km×150 km region located Southwest of France bounded to the west by the Atlantic ocean with a shoreline almost rectilinear along a north-northeast orientation. The Les Landes forest dominates the western half of the domain with 80% incorporated in the regional experiment area. It is mainly composed of maritime pines containing clearings of different sizes and are composed of agricultural land, mainly crop, and

also grassland and pasture. Historically, a plantation forest was originally planted in the area to drain the marshlands. Now, the region is managed as a commercial forest with regular harvests and crop rotations (Dolman et al., 2006).

During the measurement campaign, carbon dioxide was analyzed in the near infrared region of the electromagnetic spectrum due to its proximity to the solar Planck function maxima, which then maximizes the signal-to-noise ratio. Atmospheric oxygen was also retrieved to provide a means to determine the dry air mixing ratio, avoiding uncertainties from the surface pressure and the water vapor column. The Fourier transform spectrometer (FTS) was stationed in Biscarrosse, France at 44°22′40′N latitude, 1°13′52′W longitude and 67.6 m (above sea level) altitude. A total of 4908 spectra were analyzed during the CarboEurope regional experiment encompassing measurements from 8 May 2005 to 26 June 2005. The Bruker 120 M (Mobile) Fourier transform spectrometer was utilized during the campaign. A maximum optical path difference of 30 cm was employed and a resolution of 0.03 cm^{-1} was used. The 120 M has a focal length of 220 mm and an aperture size of 0.5 mm was used during the dates mentioned. This produces a field of view of 2.3 mrad. Forward and backward scans were taken totaling an average acquisition time of 24.0 s for each spectrum.

Beside the FTS station is a tower instrumented by the Laboratoire des Sciences du Climat et de l'Environment (LSCE). It houses a continuous in-situ monitoring station called CARIBOU, which includes a LICOR analyzer that measures CO_2 concentrations with a ±0.5 ppm precision. The tower is located at a latitude of 44°22′40.6′N, a longitude of 1°13′52.5′W with the inlet at 114.71 m (above sea level). It also houses a pressure sensor located at 106.81 m (above sea level) (Galdemard et al., 2006). Several aircraft measurements were also performed during the regional experiment. Among them is the METAIR Dimona (Dimona), a touring motor glider (TMG), in which CO_2 is measured onboard using a combination of a fast, open path LICOR 7500, a slower, more precise closed path LICOR 6262 (Neininger et al., 2001), and flask samples that are analyzed for CO_2 in the laboratory at the Max Planck Institute for Biogeochemistry (MPI-BGC) in Jena, Germany with an accuracy of 0.1 ppm. The overall precision of the

ACPD
8, 1549–1588, 2008

combined CO_2 dataset at 1 Hz is 0.5 ppm.

To aid in the interpretation of the data and to serve as a "transfer standard" between different incomparable kinds of measurements such as the FTS and the in-situ tower data, the Stochastic Time Inverted Lagrangian Transport (STILT) model was utilized (Lin et al., 2003). It is based on the HYSPLIT model (Draxler and Hess, 1997; Draxler and Hess, 1998), using a similar mean advection scheme but employing a different turbulence module. It has been further modified to use winds, surface sensible heat and momentum fluxes, and computed convective mass fluxes from ECMWF assimilated meteorological fields (Gerbig et al., 2007). Being originally designed for comparisons with in-situ measurements (single receptors or single measurement locations), STILT was modified for comparisons with column measurements (multiple receptors). The multiple receptor scheme is depicted in Fig. 1. Receptor points were placed at equal intervals along the vertical for each altitude range. The altitude ranges were set at 1–500 m, 500–3000 m, 3–6 km, 6–11 km and 11–18 km. For each receptor location, x_r, representative particles were released at a time t_r giving rise to particle densities, $\rho(x_r,t_r|\, x,t)$ at x and time t. From the particle densities, the surface influence or footprint, S(x,t), which relate surface fluxes (sources or sinks) to the concentration, C(x_r,t), at the measurement location (the receptor), can be determined. The initial boundary tracer conditions are taken from the TM3 global transport model (Heimann and Körner, 2003). For more details on the STILT model refer to the papers from Lin et al., 2003 and to Gerbig et al., 2003. The model was run at a 0.125°latitude×0.083°longitude resolution and 3 days backward in time. The CO_2 concentration output from the model (in ppm) is determined by

$$CO_2 = CO_{2,\text{background}} + CO_{2,\text{fossil;fuel}} + CO_{2,\text{photosynthetic;uptake}} + CO_{2,\text{respiration}} \quad (1)$$

where $CO_{2,\text{background}}$ is the background carbon dioxide obtained from the TM3 global transport model boundary fields, $CO_{2,\text{fossil;fuel}}$ comes from fossil fuel emissions due to combustion estimated using the recent greenhouse gas emissions inventory from the Institute of Economics and the Rational Use of Energy (IER), University of Stuttgart (http://carboeurope.ier.uni-stuttgart.de/), $CO_{2,\text{photosynthetic;uptake}}$ is the carbon dioxide

ACPD
8, 1549–1588, 2008

concentration taken up by the vegetation and $CO_{2,respiration}$ is the amount of CO_2 released by plants. The biospheric exchange is based on the diagnostic model GSB (greatly simplified biosphere) using light and temperature response and 3 vegetation classes namely forests, shrubs and crops (Gerbig et al., 2006).

3 Results

The next sections discuss results from the FTIR retrievals, comparisons with the MetAir Dimona aircraft, results from the STILT model and the effect of clouds on the retrieved O_2 and CO_2columns.

3.1 Retrieval

CO_2 and O_2 vertical columns were retrieved using the GFIT nonlinear least squares spectral fitting algorithm (version 2.40.2) developed by NASA/JPL (Toon et al., 1992). O_2 was analyzed in the 7765–8005 cm^{-1} band centered at 7885 cm^{-1} with H_2O as an interfering gas. CO_2 was retrieved in the 6180–6260 cm^{-1} band centered at 6220 cm^{-1}. Interfering gases in the 6220 cm^{-1} CO_2 band are H_2O, HDO and CH_4.

The retrieved O_2 column was compared to 20.95% of the total dry pressure column, $P_{dry,column}$. The dry pressure column was determined using

$$P_{dry,column} = \frac{P_{obs}}{m_{dry} g} - H_2O_{column} \left(\frac{m_{H_2O}}{m_{dry}} \right) \quad (2)$$

where P_{obs} is the observed surface pressure, m_{dry} is the mean molecular mass of dry air, m_{H_2O} is the mean molecular mass of water vapor, g is the density weighted acceleration due to gravity and the H_2O_{column} is the water vapor column retrieved in the O_2 window (Washenfelder et al., 2006). From this, a linear fit with zero intercept was done from which the slope (1.0432) was used to scale down the O_2 column to make it correspond with the known atmospheric O_2 concentration (0.2095). This is depicted in

ACPD
8, 1549–1588, 2008

Fig. 2. The correlation coefficient between the O_2 column and 20.95% of the total dry pressure column is 0.82. The residuals range from ±1%. The O_2 volume mixing ratio (VMR), $O_{2,vmr}$, as shown in Fig. 3, was then determined by dividing the O_2 column with the total dry pressure column. The O_2 VMR varies from 0.2061 to 0.2132.

The upper limit of the precision of the O_2 VMR was determined from its diurnal variation as shown in Fig. 4. The O_2 diurnal variation is given by

$$O_{2,diurnal} = 100 \times \left(\frac{O_{2,vmr}}{\langle O_{2,vmr} \rangle} - 1 \right) \quad (3)$$

where $\langle O_{2,vmr} \rangle$ is the daily mean of the volume mixing ratio of oxygen. One way of estimating the upper limit of the precision of CO_2 is to use the diurnal variation of the CO_2 column average VMRs (Yang et al., 2002) shown in Fig. 5. However, since there is a natural variability in the CO_2 column average volume mixing ratio over the course of the day due to diurnally varying surface sources and sinks (mostly biospheric), this method only gives an upper limit of the precision. The CO_2 diurnal variation is given as

$$CO_{2,diurnal} = 100 \times \left(\frac{CO_{2,vmr}}{\langle CO_{2,vmr} \rangle} - 1 \right) \quad (4)$$

where $CO_{2,vmr}$ is defined as 20.95% of the CO_2/O_2 column ratio for individual measurements and $\langle CO_{2,vmr} \rangle$ is the mean of the day. The CO_2/O_2 column ratio minimizes systematic errors such as errors present in the pressure and in the instrumental line shape (Warneke et al., 2005) and at the same time retaining the diurnal source/sink signals.

Quantiles were used to quantitatively assess the diurnal variations, specifically quartiles and the central 90% ile. Using quartiles, for O_2, the first quartile is at −0.2110%, the median is at 0.0007%, the third quartile is at 0.2072%, the interquartile range is 0.4182% and the quartile deviation is 0.2091%. The minimum O_2 diurnal variation is −1.6128% and the maximum O_2 diurnal variation is 1.7793%. For CO_2, the first quartile is at −0.2046%, the median is at 0.0038%, the third quartile is at 0.2098%, the

interquartile range is 0.4144% and the quartile deviation is 0.2072%. The minimum CO_2 diurnal variation is −1.2337% and the maximum CO_2 diurnal variation is 1.2826. This means that approximately 50% of the measured data have diurnal variations between ±0.21% for both O_2 and CO_2. Using the central 90% ile, for O_2, the 5% ile is at −0.5596%, the 95% ile is at 0.5558%, the 95% ile–5% ile range is 1.1154% and the central 90% ile deviation is 0.5577%. For CO_2, the 5% ile is at −0.5349%, the 95% ile is at 0.5181%, the 95% ile–5% ile range is 1.0530% and the central 90% ile deviation is 0.5265%. Approximately 90% of the measured data have diurnal variations between ±0.56% for both O_2 and CO_2. This is depicted in Fig. 6. The outliers in the diurnal variations result from influences of clouds (Warneke et al., 2006).

3.2 Aircraft comparison

The accuracy of the CO_2 retrievals was determined by comparing the FTS CO_2 VMRs with integrated aircraft carbon dioxide volume mixing ratios. Of the mentioned measurement dates, simultaneous Dimona and FTS measurements were available during five days, 25 May, 26 May, 27 May, 6 June and 14 June. During these days, only those data from the aircraft that fell within a 50 km radius from the FTS station were selected. From this, seven instances were identified wherein the Dimona and the FTS measured simultaneously with the same airmass. These instances are summarized in Table 1. The spatial coverage of the Dimona flight paths for the instances defined is shown in Fig. 7.

The Dimona reached a maximum altitude of approximately 3 km during the CarboEurope experiment. It was thus necessary to append CO_2 profiles above the aircraft ceiling. For the free troposphere portion of the profile, data were taken from the TM3 global transport model, which was coupled to surface fluxes from fossil fuel emissions as well as to the BIOME-BGC model to include biospheric exchange (Heimann and Körner, 2003). For the stratospheric part of the profile, in-situ balloon data from the Observations of the Middle Stratosphere (OMS) experiment performed in Fort Sumner, New Mexico (35° N, 104° W) on 17 September 2004 were utilized. The balloon profile was

corrected for age using the annual increase rate of CO_2. It was then coordinate transformed to potential temperature using simultaneous measurements of pressure and temperature during the balloon flight. The potential temperature was then converted to altitude using the equation formulated by Knox (1998)

$$z = \frac{\ln\left(\frac{\theta}{350}\right)}{0.045} + 13 \quad (5)$$

where θ is the potential temperature in Kelvin and z is the altitude in km. It was then converted back to pressure using NCEP altitude-pressure-temperature profiles for the specific aircraft overpass dates and the CO_2 concentration values were then interpolated. A ±0.75 ppm uncertainty was assigned based on the precision of the balloon data and on the uncertainties in the mean age of air in the stratosphere from CO_2 balloon measurements. The CO_2 concentrations for the aircraft have an uncertainty of ±0.5 ppm. For the model, a pressure dependent uncertainty in the CO_2 profile was assigned ranging from ±0.5 ppm at the aircraft ceiling increasing to a maximum of ±0.75 ppm at the tropopause.

To compare the aircraft carbon dioxide measurements with the FTS data, it is necessary to consider the different characteristics of the observing systems. Derived quantities, such as total columns, may then be compared properly among different measurement platforms. In this case, the aircraft data is said to be "simulated" by the FTS retrievals using the FTS a priori and averaging kernels (Rodgers et al., 2003). The column averaging kernels, corresponding to each instance, as well as the a priori CO_2 used in the retrievals were applied to the aircraft data using the expression

$$CO_{2,\text{simulated}} = CO_{2,a,\text{priori}} + A(CO_{2,\text{aircraft+MODEL+balloon}} - CO_{2,a\,\text{priori}}) \quad (6)$$

where $CO_{2,a,\text{priori}}$ is the a priori CO_2 profile used in the retrieval, A is the column averaging kernel (shown in Fig. 8 for instance 7) and $CO_{2,\text{aircraft+MODEL+balloon}}$ is the aircraft data appended with the model and balloon data. The simulated CO_2 profile, as shown in Fig. 8, was then integrated with respect to pressure using a trapezoidal numerical

ACPD
8, 1549–1588, 2008

integration to determine the column CO_2. The column averaged volume mixing ratio is then determined by dividing the column CO_2 by the dry pressure column.

Figure 9 shows the comparison of the averaged (retrieval error weighted) FTS CO_2 VMR (20.95% of the CO_2/O_2 column ratio) for the aforementioned instances to the integrated aircraft CO_2 VMRs. CO_2 columns were reduced by 1.0331 wherein the scaling factor was determined from the slope of a zero-intercept linear fit. The correlation coefficient is 0.69 and the residuals vary between ±1 ppm. Two instances, 4 and 6, deviated more that expected from the one-to-one line due to differences in the surface influences between the FTS and the Dimona (see Discussion).

3.3 STILT

The STILT model was used for comparison to carbon dioxide concentration time series from the Biscarrosse tower data using a single receptor placed at the same latitude and longitude as the tower with an above ground level height of 47 m. Figure 10 shows the time series comparison between STILT and the tower data. The root-mean-square (RMS) difference between the model and the measured data is 7.06 ppm. The standard deviation of the differences is 6.78 ppm and the mean difference is −1.95 ppm.

The STILT model was then extended for comparison to vertical column concentrations of CO_2 using multiple receptors along the column (see Fig. 1). Similar to what was done with the aircraft profiles, OMS in-situ balloon data, corrected for age and transformed in coordinates, were appended above the STILT model. The modeled carbon dioxide profile is shown in Fig. 11 for instance 7 compared to the Dimona-TM3-OMS CO_2 profile. The FTS retrieval a priori CO_2 and its averaging kernel were also applied (Eq. 6) to the modeled CO_2 profile before integrating the column. The column averaged VMRs of carbon dioxide from the STILT model and the FTIR data were then compared. This is shown in Fig. 12. For the STILT-FTIR comparison, the standard deviation of the differences is 0.97 ppm, the mean difference is 2.20 ppm and the correlation coefficient is 0.51. Aside from this, the column results from STILT and the FTIR data were also compared with the Weather Research and Forecasting-Vegetation Pho-

tosynthesis and Respiration Model (WRF-VPRM) modeling system. WRF-VPRM is a coupled modeling system designed to simulate high-resolution atmospheric CO_2 concentration fields. Here, WRF is the state of the art mesoscale meteorological model and it is coupled to the diagnostic biospheric model VPRM. VPRM produces biospheric CO_2 fluxes and passes to WRF, which performs atmospheric CO_2 tracer transport simulation. The modeling system also takes into account anthropogenic CO_2 fluxes. The comprehensive description of the modeling system and setup can be found in Ahmadov et al. For the WRF-VPRM-FTIR comparison, the standard deviation of the differences is 1.02 ppm, the mean difference is 3.08 ppm and the correlation coefficient is 0.24 taking note that the WRF-VPRM was not simulated by the averaging kernel and the a priori of the FTS. For the comparison between the two models, therefore, between WRF-VPRM and STILT the standard deviation of the differences is 0.652 ppm and the mean difference is −0.78 ppm.

3.4 Effect of clouds on O_2 and CO_2 precision

To quantitatively assess the effect of clouds on the precision of the retrieved O_2 and CO_2 VMRs, measurements from a clear day and a partly cloudy day during the campaign were compared. As shown in Fig. 13, 2.75-min averaged data were compared from measurements during a clear day (18 June 2005) and during a partly cloudy day (14 May 2005) characterized by thin high altitude cirrus clouds. The standard deviation of the O_2 VMR during the clear day is $\pm 3.86 \times 10^{-4}$ while for the partly cloudy is $\pm 7.44 \times 10^{-4}$. For the CO_2 VMRs, comparisons were made between the O_2 normalized carbon dioxide concentrations and the pressure normalized CO_2 vmr (CO_2 column divided by 20.95% of the dry pressure column). The standard deviation increased from ±0.62 ppm for the clear day measurement to ±1.09 ppm for partly cloudy day spectra for the O_2 normalized CO_2 volume mixing ratio while a larger increase in the standard deviation is observed for the pressure normalized CO_2 VMR from ±0.48 ppm (clear day) to ±1.31 ppm (partly cloudy day). This also shows the improved precision by normalizing with O_2 (which minimizes systematic errors) particularly for partly cloudy day

ACPD
8, 1549–1588, 2008

measurements (Washenfelder et al., 2006). These are outlined in Table 2.

4 Discussion

Surface influence functions, or footprints, which quantify the contribution of surface fluxes to the concentration of the aircraft measurement as well as of the FTIR column, can be used to assess potential reasons for disagreement between the two types of measurements. The time integrated footprints shown in Fig. 14 have been determined using STILT. They show that the surface influences for instances 4 and 6 have a significant difference for the FTS and for the Dimona aircraft. For instance 4, where the CO_2 column averaged VMR of the FTS is lower compared to Dimona (see Fig. 9, instance 4), the FTS footprint has a discontinuity in the area of northern Spain. Surface fluxes in this region would therefore not affect the FTS measurements as it does for Dimona producing the mentioned difference. This discontinuity can be attributed to particles rising above the surface hence producing no surface influence at that region. Aside from this, the aircraft is also more confined in a smaller region for this instance compared with the other instances (see Fig. 7, instance 4). This gives it a rather limited sampling area, in which other processes can influence the aircraft data as compared to the FTIR. For instance 6, the FTS column averaged VMR is higher than Dimona (see Fig. 9, instance 6). The footprints of the Dimona show more influences on land than the FTS (see Fig. 14, instance 6), consistent with the flight track covering more vegetated areas (see Fig. 7, instance 6). Given that the land region at that time of the year is a much stronger sink for CO_2 as compared to the ocean due to the active land biosphere, explains the lower CO_2 observed by the aircraft.

In Fig. 15, decomposition of the CO_2 concentration for the different altitude ranges is shown. The lower altitude ranges (1–500 m and 500–3000 m), show significant influence from the biosphere in the CO_2 variability. These altitude ranges, which are well within the planetary boundary layer where significant turbulence is experienced (hence more vertical mixing), get more contributions from vegetation photosynthetic

ACPD
8, 1549–1588, 2008

EGU

uptake and respiration. Higher up, from 3 km to 18 km, the carbon dioxide is dominated mostly by the background values with little effect from the vegetation in its variability. This also proves the point in the aircraft comparisons with the FTS that when the air masses come from the ocean, larger CO_2 is observed by the FTS compared than the aircraft which sample data along vegetation regions (instance 6) since the FTS measures carbon dioxide from areas with less biospheric influence. The altitude range and source/sink decomposition is shown in Fig. 16 for instance 6 and instances 2 and 3.

Referring to Fig. 7, one can see that there are instances (instances 4 and 6) where the Dimona was taking samples in locations where the FTS was not pointing. One might say that this could be a potential source of disagreement between the FTIR spectrometer and the aircraft. However, looking at the FTS slant and vertical column averaged VMRs in Fig. 17, one can see that taking slant or vertical column averaged VMRs does not matter. This was also verified with the WRF-VPRM also shown in Fig. 17.

The comparison between the carbon dioxide column averaged VMRs measured with the FTIR spectrometer and the MetAir Dimona aircraft can be considered to be in agreement with each other since the error bars fall within the one-to-one line (see Fig. 9). The most significant source of error for the FTS CO_2 column averaged volume mixing ratio is the precision of the instrument (120 M) used in the CarboEurope experiment. As stated earlier, the 120 M is inferior to the ones targeted and in operation for TCCON. TCCON uses more high-resolution instruments. For the integrated aircraft carbon dioxide VMR, the most significant source of uncertainty is in the spatial variability of CO_2 particularly in the planetary boundary layer (see Fig. 8). The spatial variability is a result of taking aircraft data within a 50 km radius around the FTS station. FTS and aircraft validations can therefore be improved by using higher resolutions in measuring solar absorption spectra and by flying within a closer vicinity of the FTS station.

After validating the FTS carbon dioxide column averaged VMRs with the aircraft, a meaningful next step would be to compare FTS measurements with in-situ tower

data. The problem of directly comparing in-situ and remotely sensed data is that the quantities are different in nature to start with. One needs a tool to mediate between the two measuring techniques and whose role is to assess whether both the in-situ and the FTS data are consistent with each other. This is provided by the STILT model. The comparison between the tower and STILT performed fairly well with differences partly coming from using the greatly simplified biosphere (GSB) vegetation grid in the STILT model. For the STILT-FTIR comparison, the differences is obviously not so much due to the GSB used in STILT, since STILT and WRF-VPRM agree considerably well and since column measurements are not much affected by local sources and sinks, but more due to the spatial variability in the aircraft data partly used to scale the CO_2 columns. This spatial variability is not that evident in the modeled profile (see Fig. 11). Additional information on this spatial variability will be available from the simulation of CO_2 along the flight track, however, this is beyond the scope of this paper and will be presented in a future publication focusing on the airborne data. On the other hand, the STILT model was able to capture the variability in the column averaged volume mixing ratio measured by the FTS as evidence from a relatively low standard deviation in the differences between STILT and FTIR. Both STILT and WRF-VPRM also captured the decreasing trend of CO_2 as seen from the FTS data (see Fig. 12). The decrease is part of the seasonal variation of CO_2. From Fig. 10 and Fig. 12, and from the statistics of the comparisons, STILT, which used identical model parameters for the in-situ (single receptor) and the column (multiple receptors) calculations, can therefore function as a "transfer standard" between in-situ and remotely sensed measurements.

5 Conclusions

Ground-based solar absorption measurements using Fourier transform infrared spectrometry (FTS) were performed during the CarboEurope Regional Experiment Strategy (CERES) from May to June 2005 in Biscarrosse, France. Near-infrared spectra from a Bruker 120 M FTIR spectrometer were then analyzed to retrieve carbon dioxide con-

centrations using a non-linear least squares fitting algorithm developed by NASA JPL (GFIT). The Stochastic Time Inverted Lagrangian Transport (STILT) model was used to facilitate the comparison of the FTIR CO_2 retrievals to simultaneous in-situ measurements made at a surface monitoring station and aboard an aircraft.

As an internal check on the quality of the measurements, O_2 was retrieved in the 7765–8005 cm^{-1} band. It was then compared to 20.95% of the dry pressure column resulting in a reduction factor of 1.0432 for oxygen and a correlation coefficient of 0.82. Using the diurnal variation of oxygen, the upper limit of the retrieval precision was determined. Its diurnal variation had an interquartile range of 0.4128% and its quartile deviation is 0.2091%. Its 95% ile–5% ile range is 1.1154% and its central 90% ile deviation is 0.5577%. The central 90% ile deviation shows that 90% of the retrieved O_2 columns fall within ±0.56% of the diurnal variations.

Carbon dioxide, on the other hand, was analyzed in the 6180–6260 cm^{-1} band. The diurnal variation of CO_2 had an interquartile range of 0.4144% and its quartile deviation is 0.2072%. Its 95%–5% ile range is 1.0530% and its central 90% ile deviation is 0.5265%. The retrieved carbon dioxide columns were then calibrated using data from the METAIR Dimona aircraft. Seven instances in which both the FTS and the Dimona simultaneously measured were identified. To compare the FTS and the Dimona, pressure and CO_2 model data from the TM3 global transport model and in-situ balloon data from OMS measurements were appended above the aircraft ceiling to produce CO_2 profiles during the instances. The profiles were then "simulated" using the a priori and the averaging kernels used in the FTS retrievals and were then integrated to come up with the column concentrations. The CO_2 columns were then reduced by 1.0331 after comparisons with the aircraft. The FTS and the Dimona carbon dioxide data had a 0.69 correlation coefficient. Two instances (4 and 6) deviated larger than expected from the one-to-one line and these instances were identified to have FTS and Dimona footprints that differ relatively more in terms of influence regions than the other instances. Additionally, the STILT column model outputs showed that altitudes from 0–3 km receive significant biospheric influence while altitudes above 3 km are mostly

ACPD
8, 1549–1588, 2008

affected by globally advected carbon dioxide. The difference between the slant and vertical column averaged VMRs of carbon dioxide were also analyzed and verified with the Weather Research and Forecasting - Vegetation Photosynthesis and Respiration Model (WRF-VPRM). The difference in the slant and vertical column averaged volume mixing ratio turned out to be negligible. For future FTS validation experiments using aircrafts, this means that vertical profiles should be flown in close proximity given the horizontal variability of carbon dioxide, but there is no need to adopt a slanting aircraft profile.

Time series concentrations of carbon dioxide from the STILT model were compared to in-situ tower data and to FTS column concentrations. The difference between the STILT model and the tower data partly comes from using the greatly simplified biosphere (GSB) diagnostic model that only uses 3 classes of vegetation. However, given the agreement between STILT and WRF-VPRM, another reason to consider is the scaling factor used to reduce the CO_2 columns. The scaling factor was determined from aircraft measurements that sampled at a 50 km radius from the FTS and this introduces spatial variability around the FTS. However, the variability of the column averaged VMRs measured by the FTS was modeled fairly well by STILT as seen from the calculated standard deviation between STILT and the FTIR data differences (0.97 ppm).

Since identical model parameters were used for land-atmosphere fluxes when STILT was compared with in-situ tower data (single receptor) and with column measurements from the FTS (multiple receptors), STILT can be used as a "transfer standard". Using STILT for comparing remotely sensed CO_2 data with tower measurements of carbon dioxide provided a framework that allowed validating the FTIR retrievals versus measurements made in-situ. Since these in-situ measurements are done frequently and at high accuracy on the global calibration scale, linking this scale with FTIR retrievals ultimately provides a calibration scale for remote sensing.

Acknowledgements. The authors would like to thank O. Schrems and the A. Wegener Institute for the FTS used in the campaign, P. Galdemar for the tall tower information and data, Rebecca Washenfelder for assisting in the aircraft comparisons, G. Aleks, G. Toon and P. Wennberg for

assistance and suggestions on the FTIR retrievals and B. Daube for providing OMS balloon data.

References

Ahmadov, R., C. Gerbig, R. Kretschmer, S. Koerner, B. Neininger, A., Dolman, J., and Sarrat, C.: Mesoscale covariance of transport and CO_2 fluxes: evidence from observations and simulations using the WRF-VPRM coupled atmosphere-biosphere model, J. Geophys. Res., 112, D22107, doi:10.1029/2007JD008552, 2007.

Boering, K. A., Wofsy, S. C., Daube, B. C., Schneider, H. R., Loewenstein, M., Podolske, J. R., and Conway, T. J.: Stratospheric Mean Ages and Transport Rates from Observations of Carbon Dioxide and Nitrous Oxide, Science, 274, 5291, doi:10.1126/science.274.5291.1340, 1996.

Burrows, J. P., Schneider, W., Geary, J. C., Chance, K. V., Goede, A. P. H., Aarts, H., de Vries, J. M., Smorenburg, C., and Visser, H.: Atmospheric remote sensing with SCIAMACHY, Digest of Topical Meeting on Optical Remote Sensing of the Atmosphere, Optical Society of America, Washington D. C., 4, 71, 1990.

Crisp, D., Atlas, R. M., Breon, F. M., Brown, L. R., Burrows, J. P., Ciais, P., Connor, B. J., Doney, S. C., Fung, I. Y., Jacob, D. J., Miller, C. E., O'Brien, D., Pawson, S., Randerson, J. T., Rayner, P., Salawitch, R. J., Sander, S. P., Sen, B., Stephens, G. L., Tans, P. P., Toon, G. C., Wennberg, P. O., Wofsy, S. C., Yung, Y. L., Kuang, Z., Chudasama, B., Sprague, G., Weiss, B., Pollock, R., Kenyon, D. and Schroll, S.: The orbiting carbon observatory (OCO) mission, Adv. Space Res. 34, 700–709, 2004.

Dolman, A. J., Noilhan, J., Durand, P., Sarrat, C., Brut, A., Piguet, B., Butet, A., Jarosz, N., Brunet, Y., Loustau, D., Lamaud, E., Tolk, L., Ronda, R., Miglietta, F., Gioli, B., Magliulo, V., Esposito, M., Gerbig, C., Körner, S., Glademard, P., Ramonet, M., Ciais, P., Neininger, B., Hutjes, R. W. A., Elbers, J. A., Macatangay, R., Schrems, O., Pérez-Landa, G., Sanz, M. J., Scholz,Y., Facon, G., Ceschia, E., and Beziat, P.: The CarboEurope Regional Experiment Strategy, Am. Meteorol. Soc., 87, 1367–1379, 2006.

Draxler, R. R. and Hess, G. D.: Description of the HYSPLIT_4 modeling system, NOAA Tech. Memo, ERL ARL-224, 24 pp, 1997.

Draxler, R. R. and Hess, G. D.: An overview of the HYSPLIT_4 modelling system for trajectories, dispersion, and deposition, Aust. Meteorol. Mag., 47, 295–308, 1998.

Dufour E., Bréon, F., and Peyling, P.: CO_2 column averaged mixing ratio from inversion of ground-based solar spectra, J. Geophys. Res., 109, D09304, doi:10.1029/2003JD004469, 2004.

Galdemard, P., Ramonet, M., Schmidt, M., Ciais, P., Jourd'heuil, L., Arranger, D., Allard, J., Azoulay, R., Bargueden, P., Beauvais, P., Belorgey, J., Boussuge, O., Cloué, P., Contrepois, P., De Antoni, P., Durand, G. A., Eppellé, D., Jannin, J. L., Joubert, J. M., Le Noa, Y., Noury, J., Massinger, M., Séguier, P., Walter, C., Bhatt, B. C., and Vinod Gaur, K.: CARIBOU: New Instruments for Continuous CO_2 Measurements and On-line Data Transmission, Proc. of the 13th WMO/IAEA Meeting of Experts on Carbon Dioxide Concentration and Related Tracer Measurement Techniques, Boulder, Colorado, USA, 19–22 September 2005, WMO-GAW Report 168, edited by: Miller, J. B., 83–89, December 2006.

Gerbig, C., Körner, S., and Lin, J. C.: Vertical mixing in atmospheric tracer transport models: error characterization and propagation, Atmos. Chem. Phys. Discuss., 7, 13 121–13 150, 2007.

Gerbig, C., Lin, J. C., Munger, J. W., and Wofsy, S. C.: What can tracer observations in the continental boundary layer tell us about surface-atmosphere fluxes?, Atmos. Chem. Phys., 6, 539–554, 2006, http://www.atmos-chem-phys.net/6/539/2006/.

Gerbig, C., Lin, J. C., Wofsy, S. C., Daube, B. C., Andrews, A. E., Stephens, B. B., Bakwin, P. S., and Grainger, C. A.: Toward constraining regional-scale fluxes of CO_2 with atmospheric observations over a continent: 2. Analysis of COBRA data using a receptor-oriented framework, J. Geophys. Res., 108(D24), 4757, doi:10.1029/2003JD03770, 2003.

Heimann, M. and Körner, S.: The Global Atmospheric Tracer Model, TM3, Model Description and Users Manual Release 3.8a, No. 5, Max Planck Institute for Biogeochemistry (MPI-BGC), Jena, Germany, 2003.

IPCC, Mertz, B., Davidson, O., de Coninck, H., Loos, M., and Meyer, L.: IPCC Special Report on Carbon Dioxide Capture and Storage, Cambridge University Press, New York, USA, 2005.

Knox, J. A.: On converting potential temperature to altitude in the middle atmosphere, Eos Trans., 79(31), 376, 1998.

Lin, J. C., Gerbig, C., Wofsy, S. C., Andrews, A. E., Daube, B. C., Davis, K. J., and Grainger, C.

A.: A near-field tool for simulating the upstream influence of atmospheric observations: The Stochastic Time-Inverted Lagrangian Transport (STILT) model, J. Geophys. Res., 108(D16), 4493, doi:10.1029/2002JD003161, 2003.

McCartney, E.: Absorption and Emission by Atmospheric Gases: The Physical Processes, John Wiley & Sons, Inc., USA, 2–7, 1983.

Neininger, B., Fuchs, W., Baeumle, M., Volz-Thomas, A., Prévôt, A. S. H., and Dommen, J.: A Small Aircraft for More than Just Ozone: METAIR's "Dimona" After Ten Years of Evolving Development, Proc. of the 11th Symposium on Meteorological Observations and Instrumentation, 81st AMS Annual Meeting, 14–19 January 2001, Albuquerque, NM, USA, 123–128, 2001.

Peters, W. Jacobsen, A .R., Sweeney, C., Andrews, A. E., Conway, T. J., Masarie, K., Miller, J. B., Bruhwiler, L. M. P., Petron, G., Hirsch, A. I., Worthy, D. E. J., van der Werf, G. R., Randerson, J. T., Wennberg, P. O., Krol, M. C., and Tans, P. P.: An atmospheric persepective on North America carbon dioxide exchange: CarbonTracker, P. Natl. Acad. Sci. USA, 104, 18 925–18 930, 2007.

Peylin, P., Bousquet, P., Le Qu'er'e, C., Sitch, S., Friedlingstein, P., McKinley, G., Gruber, N., Rayner, P., and Ciais, P.: Multiple constraints on regional CO_2 flux variations over land and oceans, Global Biogeochem. Cy., 19, GB1011, doi:10.1029/2003GB002214, 2005.

Rodgers, C. D. and Connor, B. J.: Intercomparison of remote sounding instruments, J. Geophys. Res., 108(D3), 4116, doi:10.1029/2002JD002299, 2003.

Rödenbeck, C., Conway, T. J., and Langenfelds, R. L.: The effect of systematic measurement errors on atmospheric CO_2 inversions: a quantitative assessment, Atmos. Chem. Phys., 6, 149–161, 2006, http://www.atmos-chem-phys.net/6/149/2006/.

Sarrat, C., Noilhan, J., Lacarrère, P., Donier, S., Lac, C., Calvet, J. C., Dolman, A. J., Gerbig, C., Neininger, B., Ciais, P., Paris, J. D., Boumard, F., Ramonet, M., and Butet, A.: Atmospheric CO_2 modeling at the regional scale: Application to the CarboEurope Regional Experiment, J. Geophys. Res., 112, D12105, doi:10.1029/20067JD008107, 2007.

Toon, G. C., Farmer, C. B., Schaper, P. W., Lowes, L. L., Norton, R. H.: Composition Measurements of the 1989 Arctic Winter Stratosphere by Airborne Infrared Solar Absorption Spectroscopy, J. Geophys. Res., 97, doi:10.1029/91JD03114, 1992.

Warneke, T., Yang, Z., Olsen, S., Körner, S., Notholt, J., Toon, G., Velazco, V., Schulz, A., and Schrems, O.: Seasonal and latitudinal variations of column averaged volume-mixing ratios

of atmospheric CO_2, Geophys. Res. Lett., 32, L03808, doi:10.1029/2004GL021597, 2005.
Warneke, T., Meirink, J. F., Bergamaschi, P., Grooß, J.-U., Notholt, J., Toon, G. C., Velazco, V., Goede, A. P. H., and Schrems, O.: Seasonal and latitudinal variations of atmospheric methane: A ground-based and ship-borne solar IR spectroscopic study, Geophys. Res. Lett., 33, L14812, doi:10.1029/2006GL025874, 2006.
Washenfelder, R. A., Toon, G. C., Blavier, J.-F., Yang, Z., Allen, N. T., Wennberg, P. O., Vay, S. A., Matross, D. M., and Daube, B. C.: Carbon dioxide column abundances at the Wisconsin Tall Tower site, J. Geophys. Res., 111, D22305, doi:10.1029/2006JD07154, 2006.
Waugh, D. W. and Hall, T. M.: Age of stratospheric air: Theory, observations, and models, Rev. Geophys, 40(4), 1010, doi:10.1029/2000RG000101, 2002.
Yang, Z., Toon, G. C., Margolis, J. S., and Wennberg, P. O.: Atmospheric CO_2 retrieved from ground-based near IR solar spectra, Geophys. Res. Lett., 29(9), 1339, doi:10.1029/2001GL014537, 2002.

Table 1. Instances. Dates and times where both the MetAir Dimona aircraft and the FTS had measurements.

Instance	Date	Time (UTC)	Max. Altitude of Dimona (km)
1	25 May	10:00–13:00	2.7249
2	26 May	10:00–11:00	3.0655
3	26 May	13:00–15:00	2.5573
4	27 May	07:00–09:00	3.2324
5	27 May	12:00–14:00	2.6851
6	6 June	09:00–13:00	2.5615
7	14 June	10:00–15:00	2.6441

Table 2. Clear and Partly Cloudy Days (2.75-min averages). Normalizing CO_2 by O_2 increases the precision particularly for partly cloudy days.

	18 June (Clear Day)	14 May (Partly Cloudy Day)
O_2 VMR	$0.2095 \pm 3.86 \times 10^{-4}$	$0.2096 \pm 7.44 \times 10^{-4}$
CO_2 VMR (O_2 Normalized)	377.52±0.62 ppm	379.37±1.09 ppm
CO_2 VMR (Pressure Normalized)	377.55±0.48 ppm	379.61±1.31 ppm

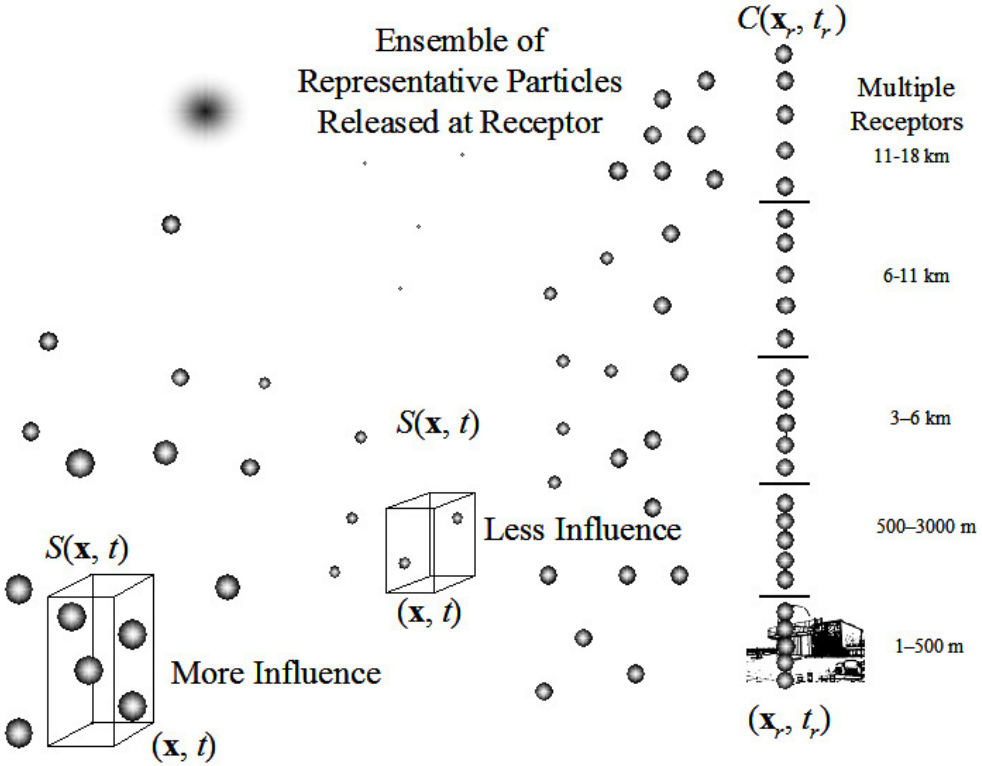

Fig. 1. STILT Applied to Column Measurements. Receptor points were placed at equal intervals along the vertical column for each altitude range. Altitude ranges are from 1–500 m, 500–3000 m, 3–6 km, 6–11 km and 11–18 km. The released particles give rise to particle densities at certain locations wherein influences can be calculated.

ACPD
8, 1549–1588, 2008

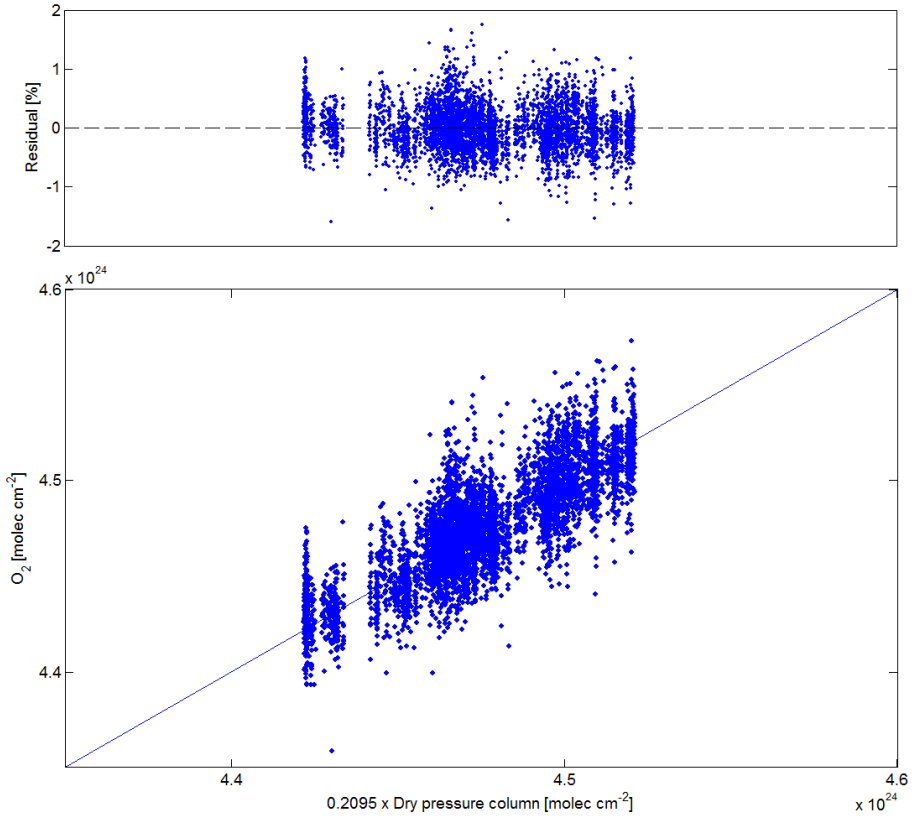

Fig. 2. Comparison of the O_2 column with 20.95% of the total dry pressure column. The correlation coefficient is 0.82. A line of slope 1.0432 with zero intercept was fitted to the data and this slope was used to reduce the O_2 column to make it correspond with the known O_2 concentration of 0.2095.

ACPD
8, 1549–1588, 2008

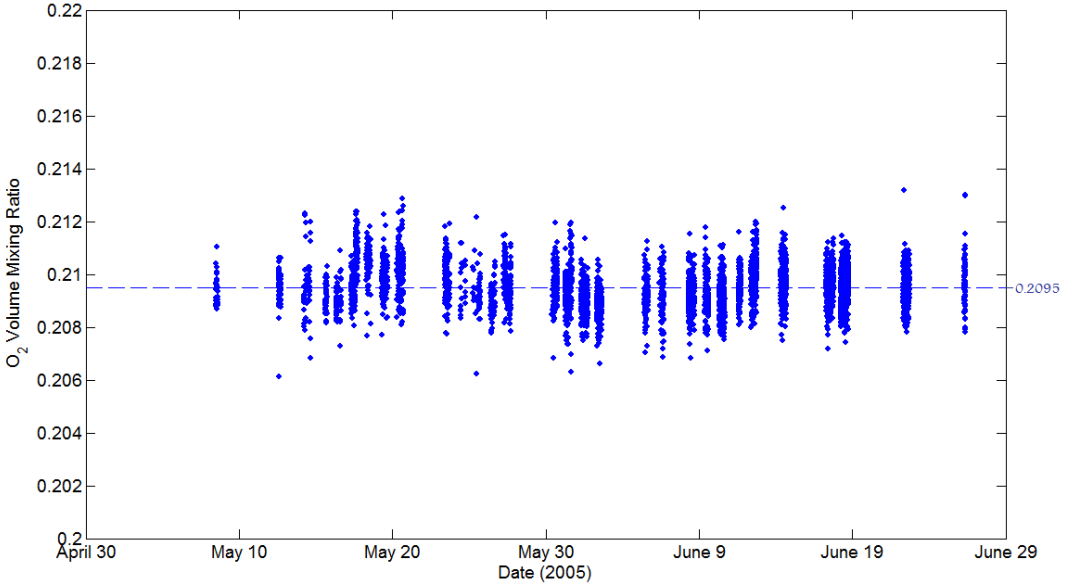

Fig. 3. O_2 Volumn Mixing Ratio. The O_2 vmr varies from 0.2061 to 0.2132.

ACPD
8, 1549–1588, 2008

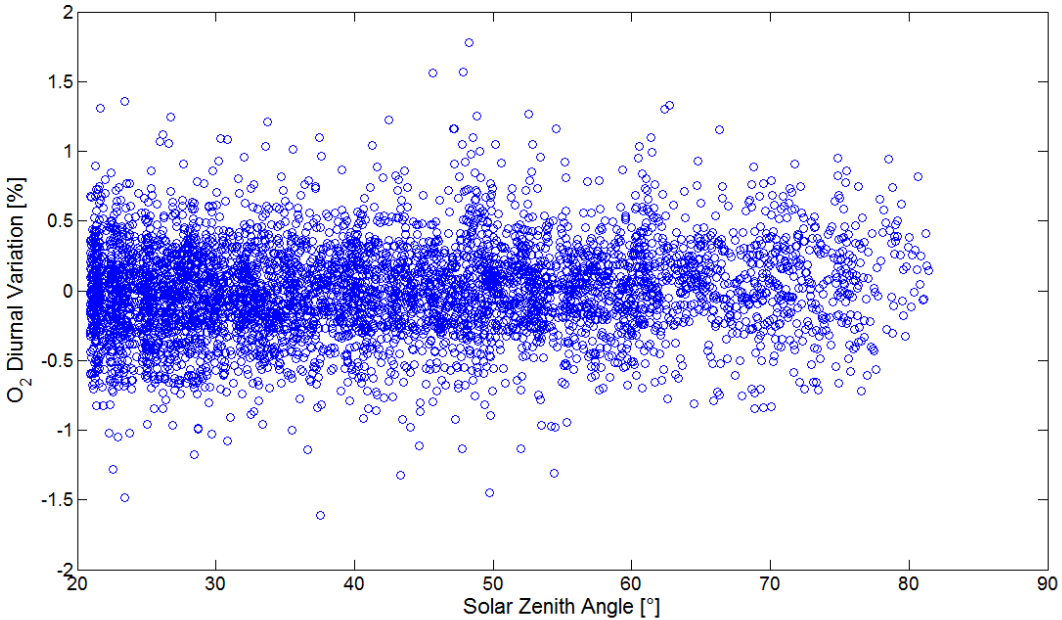

Fig. 4. O_2 Diurnal Variation.

ACPD
8, 1549–1588, 2008

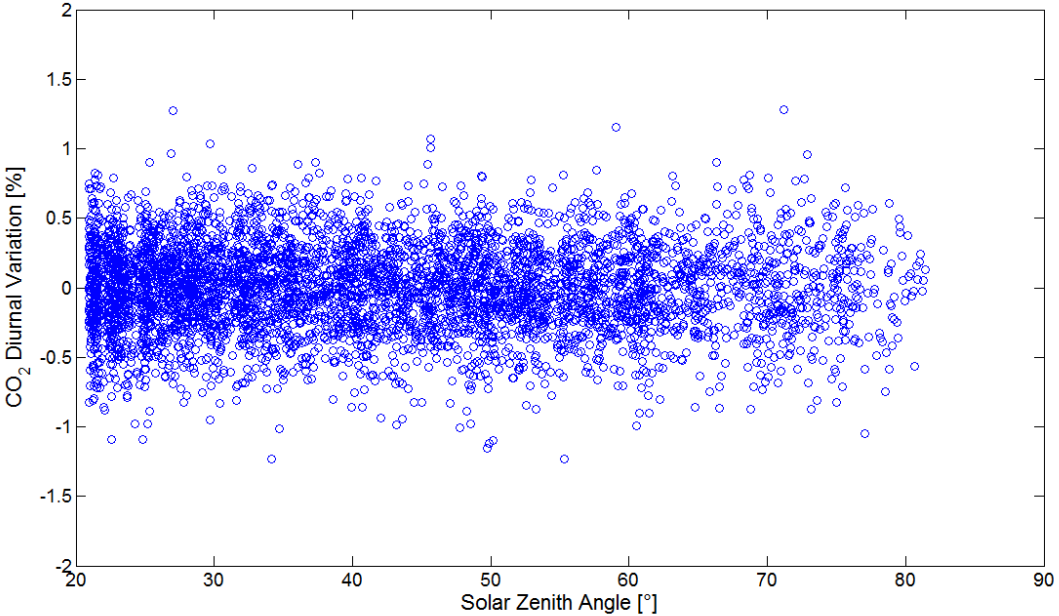

Fig. 5. CO_2 Diurnal Variation.

ACPD
8, 1549–1588, 2008

EGU

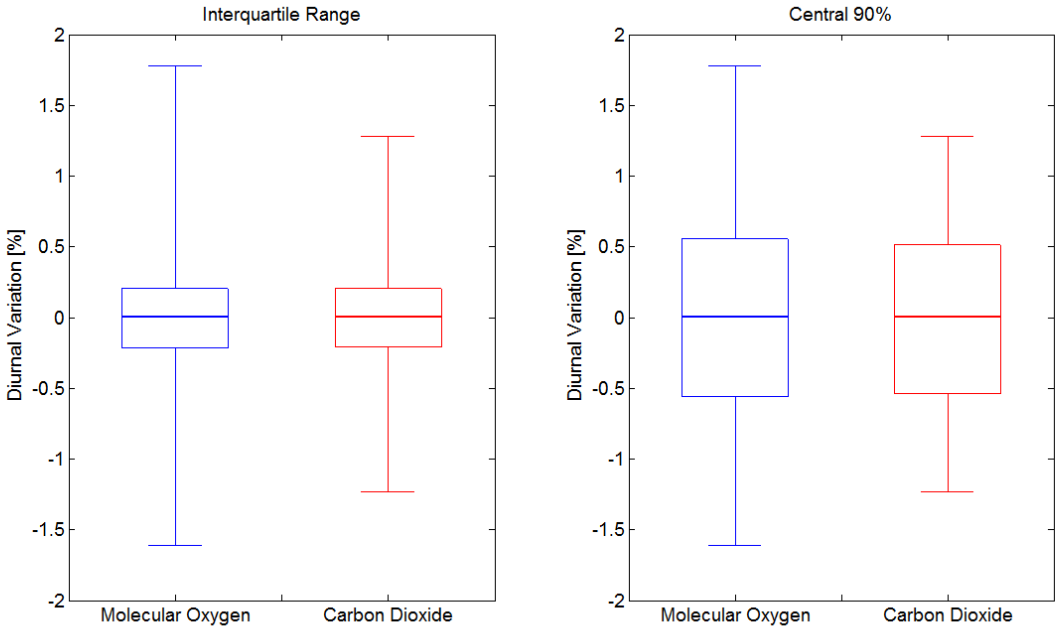

Fig. 6. Quantiles of the Diurnal Variations of O_2 and CO_2.

ACPD
8, 1549–1588, 2008

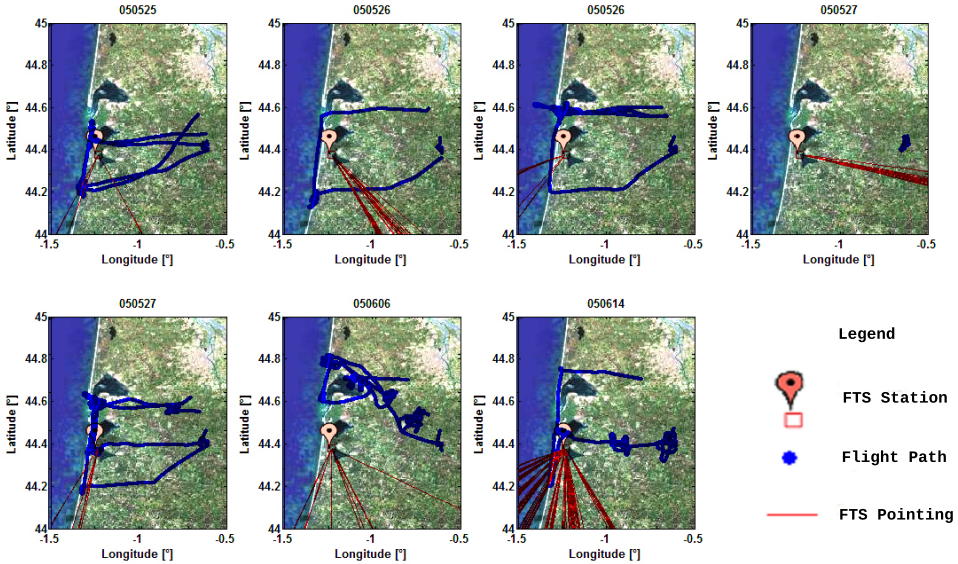

Fig. 7. Spatial Coverage. Shown is the location of the FTS station, the flight paths of the MetAir Dimona and the direction where the FTS was pointing for instances 1–7.

ACPD
8, 1549–1588, 2008

EGU

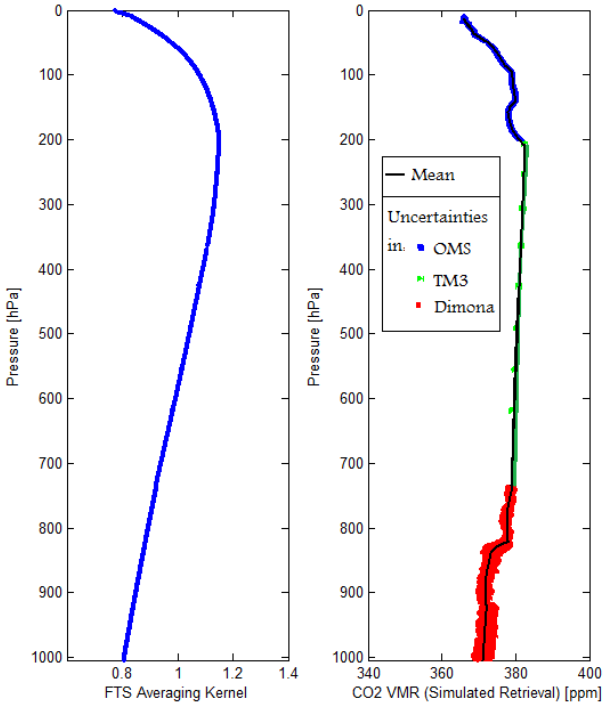

Fig. 8. CO_2 Profile for Instance 7 (14 June 2005; 10:00–15:00 UTC). (Left) The averaging kernel used in the FTS retrieval was applied to the aircraft data to make a comparison with the Fourier transform spectrometer CO_2 concentration data using the expression $CO_{2,simulated}=CO_{2,a,priori} + A(CO_{2,aircraft+MODEL+balloon} - CO_{2,a,priori})$. (Right) Simulated CO_2 profile after pressure and CO_2 concentrations from the TM3 global transport model and from OMS in-situ balloon data were appended above the aircraft ceiling. CO_2 concentration data for the aircraft have an uncertainty of ± 0.5 ppm. Above the aircraft ceiling, the modeled CO_2 data was assigned to have a pressure dependent uncertainty varying from ±0.5 ppm to ±0.75 ppm. The uncertainty in the balloon data was estimated to have a ±0.75 ppm based upon the variability of the measured CO_2 data and the mean age of air in the stratosphere.

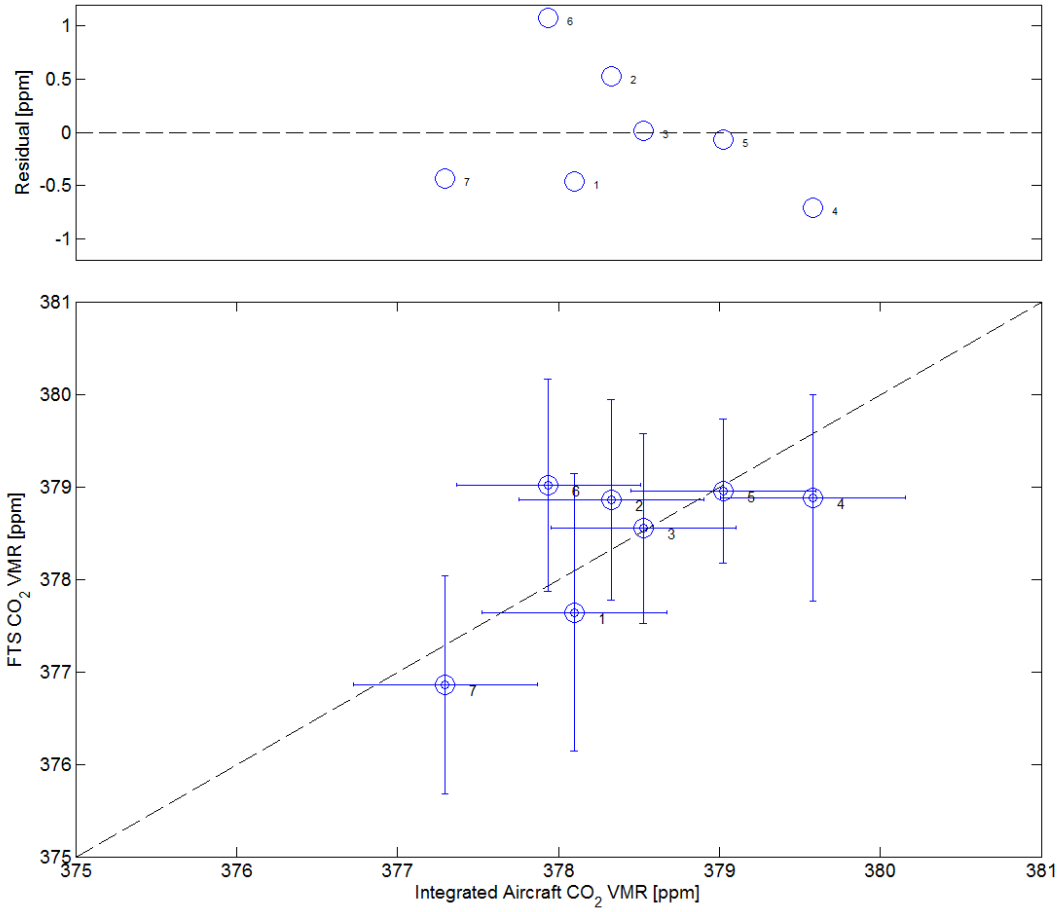

Fig. 9. FTS and Integrated Aircraft CO_2 Comparison. CO_2 columns were reduced by 1.0331 determined from the slope of a zero intercept linear fit. The correlation coefficient is 0.69 and the residuals vary between ±1 ppm.

ACPD
8, 1549–1588, 2008

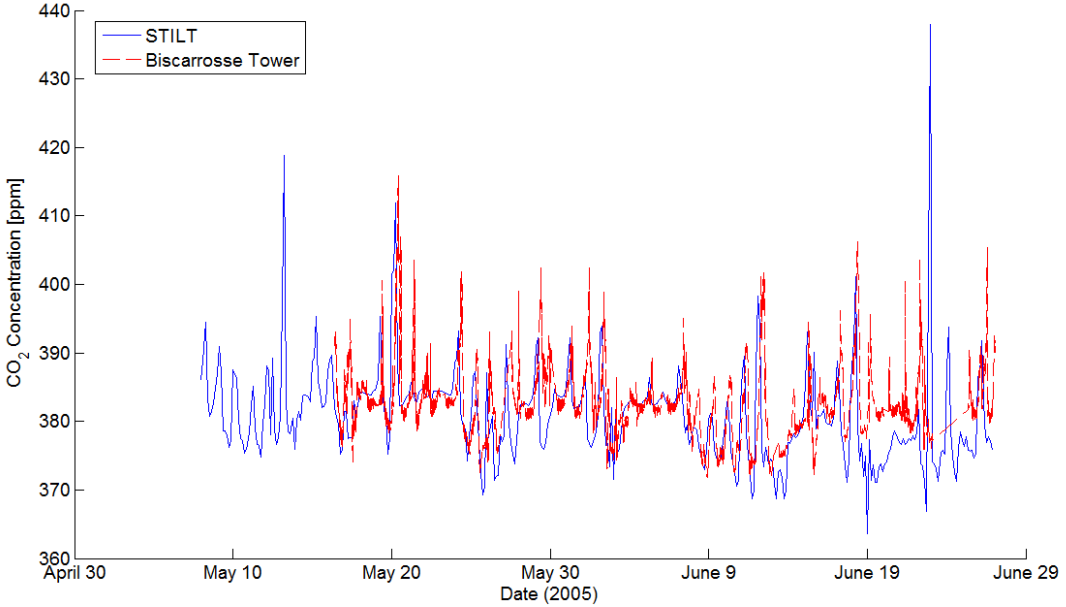

Fig. 10. STILT-Biscarrosse Tower Comparison. The RMS of the differences between the two data sets is 7.06 ppm, the standard deviation of the differences is 6.78 ppm and the mean difference is −1.95 ppm.

ACPD
8, 1549–1588, 2008

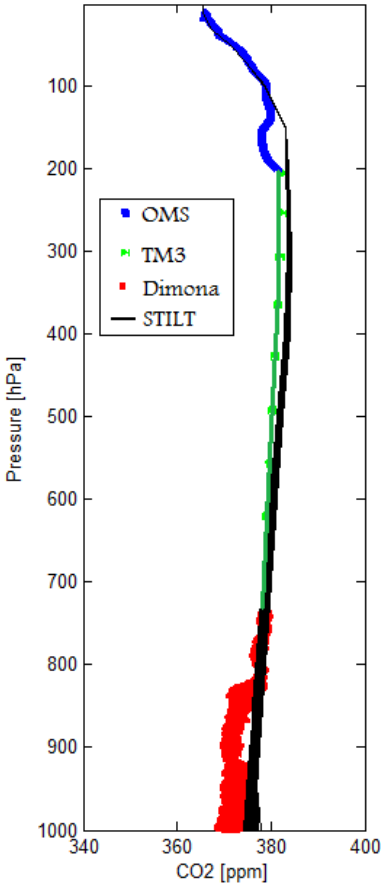

Fig. 11. Dimona-TM3-OMS and STILT Carbon Dioxide Profiles for Instance 7.

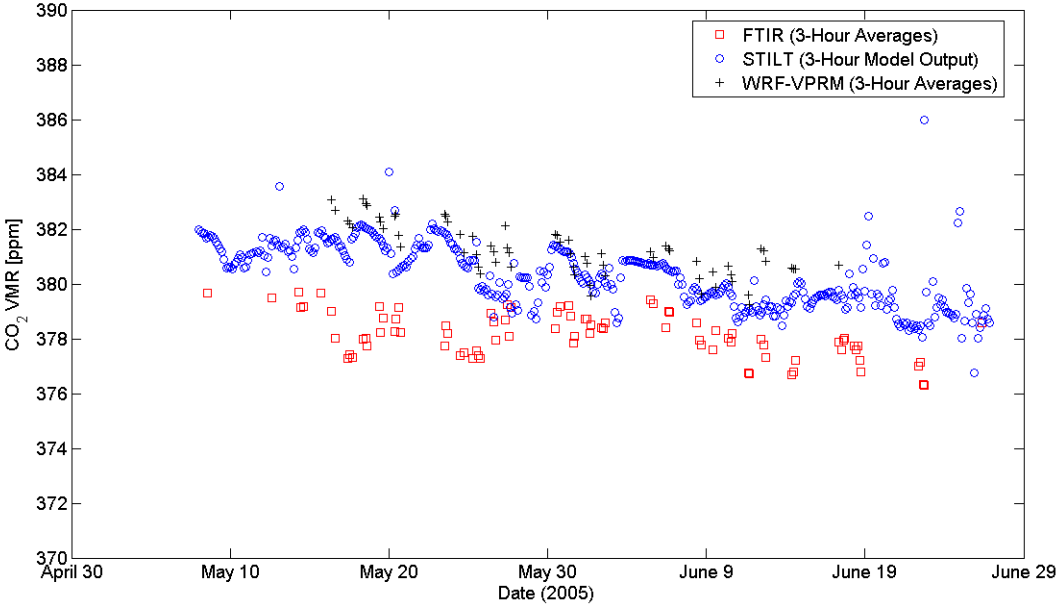

Fig. 12. STILT, WRF-VPRM and FTIR Comparisons.

ACPD
8, 1549–1588, 2008

EGU

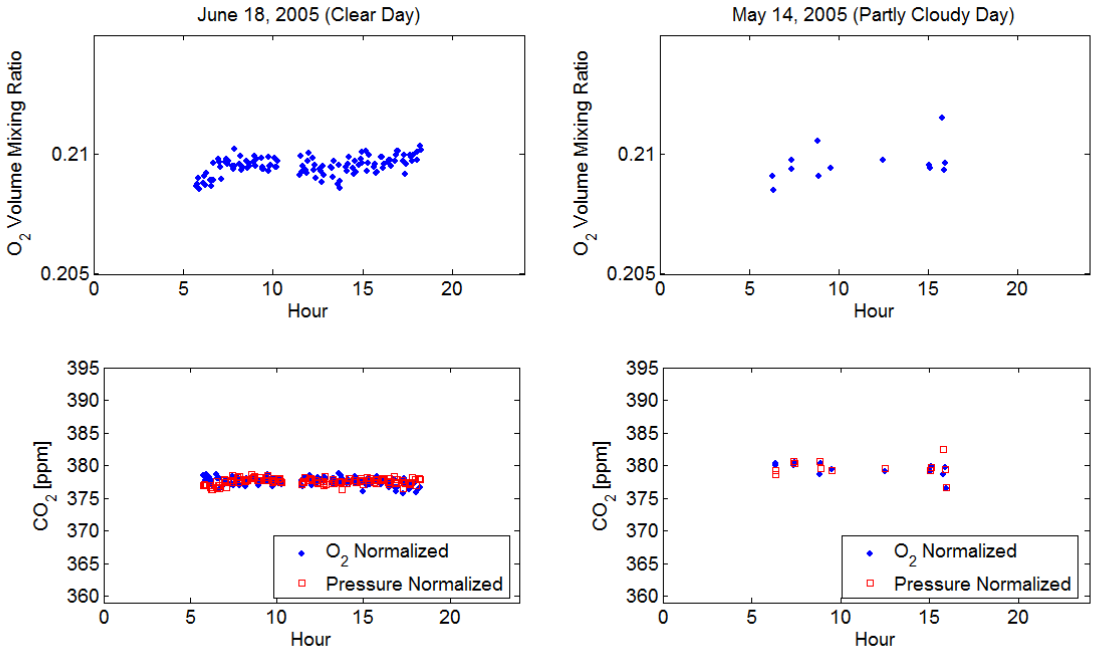

Fig. 13. Clear and Partly Cloudy Days (2.75-min averages). Thins cirrus clouds affect the precision of both O_2 and CO_2 VMRs.

ACPD
8, 1549–1588, 2008

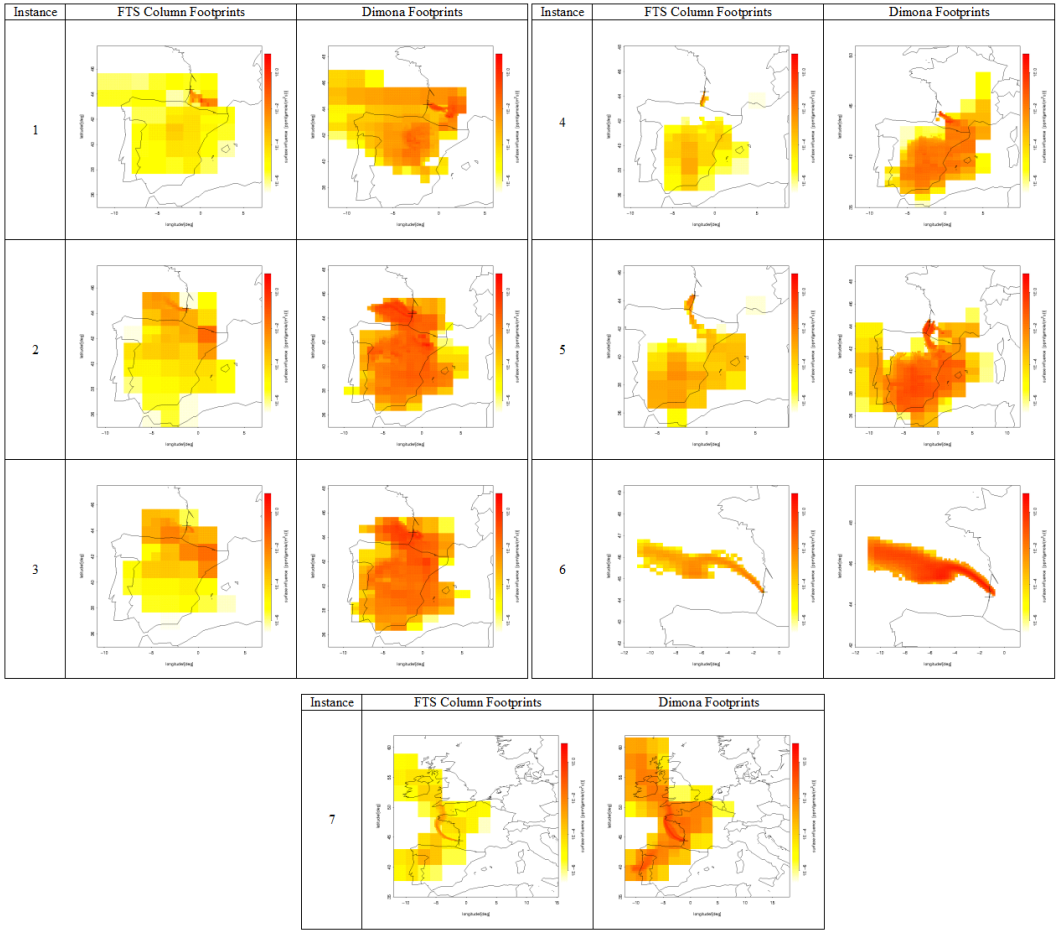

Fig. 14. Footprints for Instances 1 to 7. Instances 4 and 6 footprints have a significant difference between the FTS and the Dimona explaining their larger than expected deviation from the one-to-one line.

ACPD
8, 1549–1588, 2008

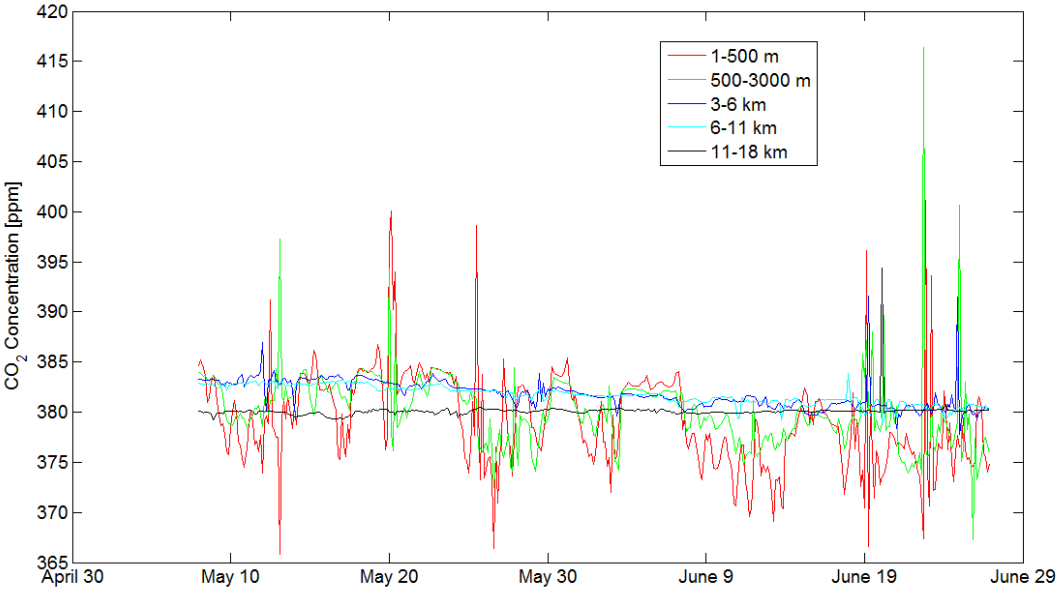

Fig. 15. STILT Decomposition of CO_2 by Altitude Range. The CO_2 multiple receptor signal is decomposed into the different altitude ranges of 1–500 m, 500–3000 m, 3–6 km, 6–11 km and 11–18 km.

ACPD
8, 1549–1588, 2008

EGU

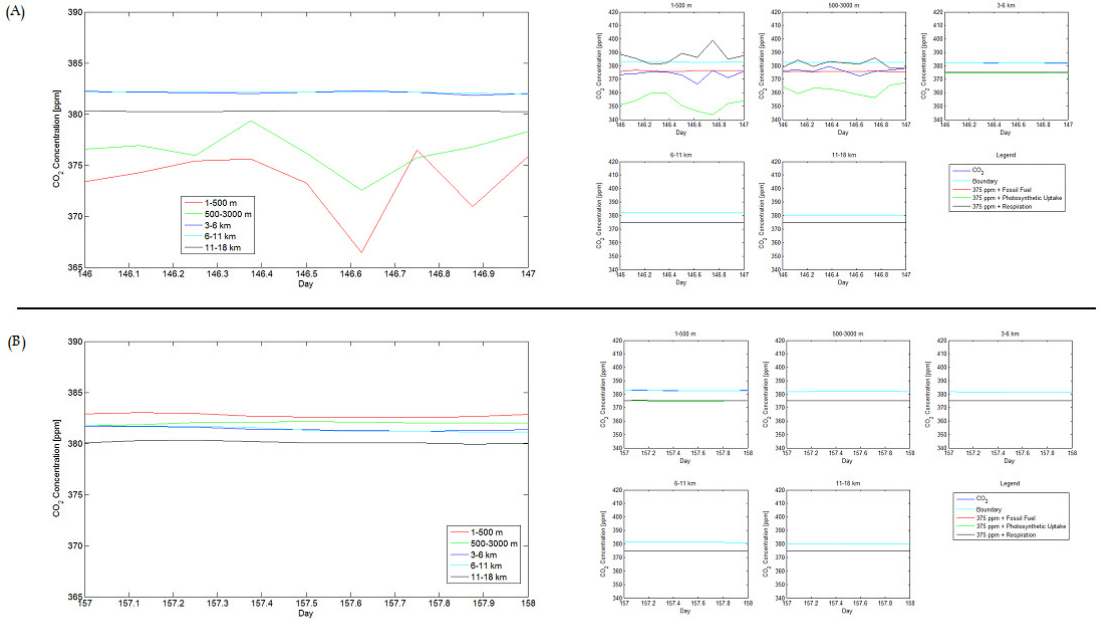

Fig. 16. STILT Decomposition of CO_2 by Altitude Range and Sources/Sinks for **(A)** Instances 2, 3 and **(B)** Instance 6. Instance 6 receives less influence form the biosphere since the footprints originate mostly from the ocean. This produces a higher CO_2 value detected by the FTS than the aircraft (sampling over vegetation).

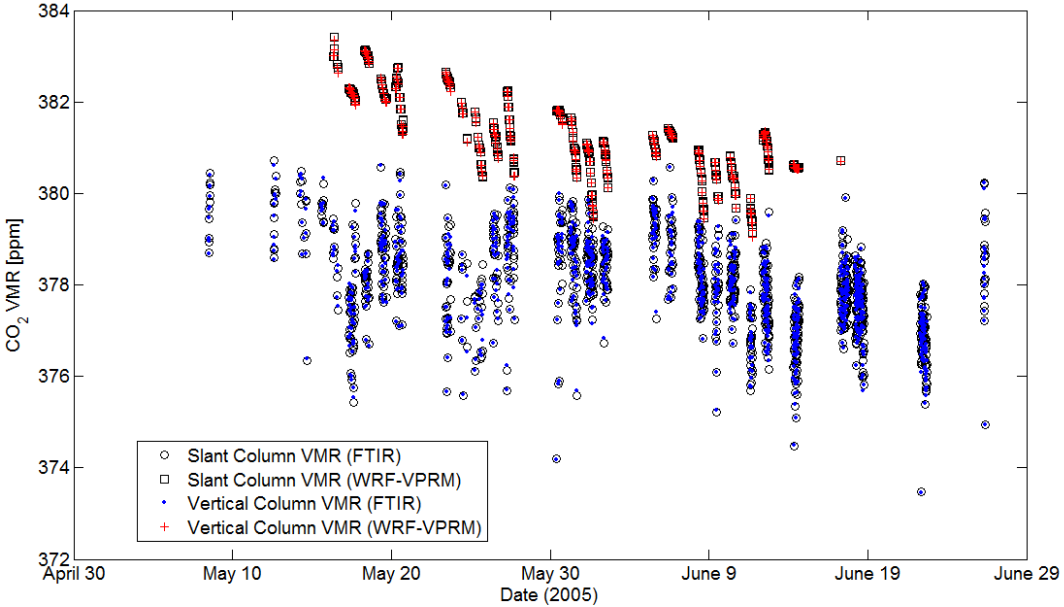

Fig. 17. 2.75-min averaged Slant and Vertical Columns from the FTS and the WRF-VPRM Model.

ACPD
8, 1549–1588, 2008

EGU